## Title

Ion—surface interactions in plasma-facing material design



## Journal

Journal of Applied Physics, 135(18)

## ISSN

0021-8979

## Authors

Sabiston, Graeme
Wirz, Richard E

## Publication Date

2024-05-14

## DOI

10.1063/5.0201758

Journal of Applied Physics

RESEARCH ARTICLE | MAY 10 2024

# Ion–surface interactions in plasma-facing material design

Graeme Sabiston ; Richard E. Wirz



*J. Appl. Phys.* 135, 183301 (2024)
https://doi.org/10.1063/5.0201758

Journal of Applied Physics ARTICLE pubs.aip.org/aip/jap

# Ion–surface interactions in plasma-facing material design

Cite as: J. Appl. Phys. **135**, 183301 (2024); doi: 10.1063/5.0201758
Submitted: 31 January 2024 · Accepted: 12 April 2024 ·
Published Online: 10 May 2024

View Online Export Citation CrossMark

Graeme Sabiston[1,a] and Richard E. Wirz[1,2,b]

## AFFILIATIONS

[1]Mechanical and Aerospace Engineering, University of California, Los Angeles, 420 Westwood Plaza, Los Angeles, California 90095, USA
[2]Aerospace Research Program, Oregon State University, 221 Dearborn Hall, Corvallis, Oregon 97331, USA

[a]**Electronic mail:** graemes1@ucla.edu
[b]**Author to whom correspondence should be addressed:** richard.wirz@oregonstate.edu, wirz@ucla.edu

## ABSTRACT

A multi-scale simulation framework for ion–solid interactions in plasma-exposed materials provides crucial insight into advancing fusion energy and space electric propulsion. Leveraging binary-collision approximation (BCA) simulations, the framework uniquely predicts sputter yields and analyzes material transport within volumetrically complex materials. This approach, grounded in the validated BCA code TRI3DYN, addresses key limitations in existing models by accurately capturing ion–solid interaction physics. A case study is presented, highlighting the framework's ability to replicate experimental sputter yield results, underscoring its reliability and potential for designing durable materials in harsh plasma environments. Insights into sputtering transport phenomenology mark a significant advancement in material optimization for improved resilience in plasma-facing applications.





## I. INTRODUCTION

Anticipated breakthroughs in fusion energy and space electric propulsion (EP) in the coming decades will likely be tied to parallel advancements in the ability of materials to endure the harsh plasma-facing conditions that these systems produce.[1–4] Finding materials that are capable of withstanding these environments is critical for the development of high-power cathodes, such as those found in Z-pinch fusion reactors, or magnetoplasmadynamic thrusters, as well as enabling more resilient first-wall materials for tokamak fusion reactors or plasma-exposed space propulsion devices.

One of the main erosion mechanisms in EP thrusters and fusion reactors that limit lifetime is known as physical sputtering. This process occurs when energetic ions in a plasma collide with a material, transferring their energy to the surface atoms and dislodging them into the bulk plasma.[5] Most studies on sputtering transport have focused on understanding how flat and featured surfaces experience erosion, leaving limited research on how complex three-dimensional structures react to plasma exposure.

### A. Volumetrically complex materials

Researchers in the Plasma, Energy, and Space Propulsion Lab (PESPL) at the University of California, Los Angeles (UCLA) have developed a new class of materials to directly address the aforementioned plasma–material interaction challenges. Volumetrically complex materials (VCMs) are novel open-cell structures that have been experimentally proven to be up to ten times more robust to sputtering in harsh plasma environments, with the implied potential to significantly increase the lifetime of critical fusion and space propulsion components.[6–14] Figure 1 depicts a stochastic foam-like aluminum VCM experiencing plasma sputtering erosion in the Plasma Interaction (Pi) Facility at UCLA. While the majority of the VCM research to date has been related to stochastic foams, the concept of a VCM extends to intentionally designed and manufactured complex geometric structures. VCMs exhibit a "bend-but-don't-break" advantage by absorbing the energetic species of the plasma without catastrophic micro-scale cracking and sputtering, and macro-scale failures that occur in conventional materials.

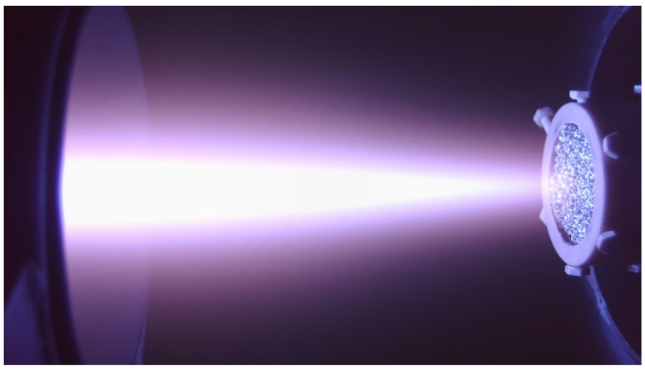

**FIG. 1.** Plasma interacting with aluminum stochastic foam VCM in the Plasma Interaction (Pi) Facility at UCLA.

The primary mechanism of sputter-resistance in VCMs under plasma-facing conditions can be described as follows: While the ligaments of a VCM are subject to sputtering, a significant portion of the dislodged atoms from these ligaments re-adhere to adjacent ligaments before they can leave the structure. This phenomenon is known in the literature as geometric trapping.

While empirical experiments are undeniably valuable, the intricate design space and multitude of potential applications for VCMs underscore the need for a robust simulation tool. Such a tool would not only streamline the testing of these materials for sputter-resistance but also offer predictive capabilities essential for the rapid advancement of plasma-exposed materials.

### B. Sputtering erosion simulations

VCMs have minimum feature sizes in the range of hundreds of micrometers, while their unit cell geometries can be on the order of ten millimeters; any computational tool should be well equipped to simulate sputtering across these length scales. While there exist many computational efforts that describe sputter erosion mechanisms on small scales, using techniques such as molecular dynamics (MD),[15–19] or binary-collision approximation (BCA),[20–23] there is an absence of rigorous studies aimed at developing simulation tools specifically for the modeling of sputtering phenomena on macroscopic length-scales. One such exception is a Monte Carlo ray-tracing algorithm reported by Nadvornick *et al.*,[24] which provides insights into the transport and evolution of structures under sputtering erosion. However, there exist some assumptions that may potentially lead to inaccurate sputter yield calculations. First, the authors utilize the probability distribution functions (PDFs) of particle trajectory derived from the ion–solid interaction code known as transport of ions in matter (TRIM),[23] approximating a cosine distribution. TRIM has been proven to provide highly inaccurate probability distribution functions of ejected sputtered particles that remain largely cosine in behavior, independent of ion energy and incidence angle due to unresolved computational issues in the code itself.[25–28] Other studies that utilize more advanced BCA codes show much more asymmetric PDFs across a wide range of incidence angles and ion energies, which agree with the experiment.[25,29] Additionally, it appears as though analytical functions have been invoked to calculate sputter yield; however, these functions result in non-integer sputter yield values, which cannot be realized in a discrete ray-tracing environment. Therefore, there exists a need for a computational framework that addresses these issues and, furthermore, provides an environment in which sputter-reducing candidate geometries can be rapidly generated, simulated, iterated upon, and optimized.

### C. Study objective

The lack of sputtering simulation tools for large-scale geometries is primarily due to the fact that the computational expense required to complete MD or BCA simulations for structures on the scale of centimeters is prohibitive. Therefore, a reduced-order model that captures the relevant physics with a manageable computational overhead is required. The goal of this study is to develop multi-scale modeling that utilizes BCA-informed sputtering dynamics, and performs particle tracking of sputtered species to enable characterization of VCM behavior and performance. The simulation environment has been constructed with optimization in mind, as candidate geometries can be parametrically constructed and gradient-based methods can be used to search the broad design space to achieve minimal sputtering designs for volumetrically complex materials. The authors seek to provide deeper insights into ion–surface interactions and sputterant transport, ultimately leading to more accurate material design predictions to enhance the performance and longevity of plasma-facing materials.

## II. ION–SOLID INTERACTION THEORY AND SIMULATION

The field of study known as ion–solid interaction examines the interplay of projectiles with solid or gas target structures based on quantum-mechanical arguments, at energies ranging from a few eV to greater than 1 MeV.[30,31] Incident particles (usually singly charged ions) cause a host of damage phenomena in targets, such as recoil atoms (primary, secondary, etc.), vacancies, and sputtered atoms (Fig. 2, left). The governing forces for these motions are derived from interaction potentials between atomic nuclei, while accounting for the effects of electron excitation. Shown in Fig. 2 (right), scattering integrals are constructed based on the choice of interaction potential, incident projectile energy, and binding energy of the target atom, among other factors.

### A. Oblique incidence yield dependence

A well-known behavior of ion–solid interactions is the marked increase in sputtering as the angle of incidence is increased from normal (defined as 0°) to grazing; this behavior is generally independent of projectile–target combination.[32] This is due to the projectile being able to more readily deposit its energy into the initial layers of the target, rather than into deeper layers, which have little contribution to sputtering. Increases of twofold are common, with some material combinations and projectile energies surpassing fivefold. The peak of sputter yield has been found to typically be

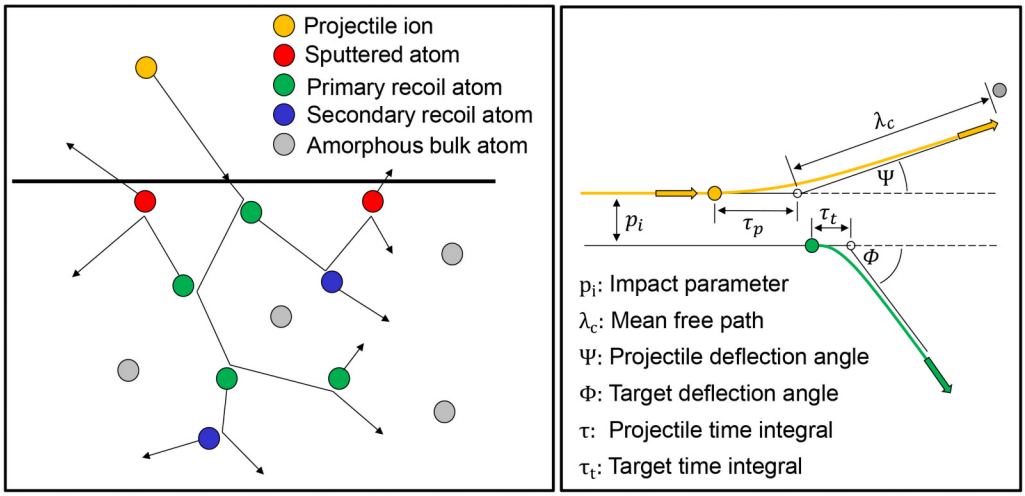


**FIG. 2.** Left: Straight line collision cascade caused by an incident ion striking amorphous target material, and the varying species of recoil atoms that are generated. Right: Scattering geometry for a projectile/recoil atom pair, with important collision parameters included for reference.

around 70° incidence angle and falls off precipitously with higher grazing angles as the projectiles are conversely less able to effectively transfer energy to the surface atoms beyond a certain threshold (see Fig. 3). Through experimental evidence, it is generally observed that the structure of a surface determines the glancing angle at which the surface atoms' repulsive force becomes powerful enough to impede the penetration of ions into the target.[33]

### B. Probability distribution functions

The trajectories of sputtered atoms after leaving the target surface are of high importance as this information can help predict preferential directions in which sputtered particles are likely to accumulate. At low energies (100–500 eV) and normal incidence, a characteristic symmetric under-cosine, or "butterfly" PDF pattern emerges, with the majority of sputtered atoms being ejected to the sides, with a minimum arising in the center.[35] As shown in Fig. 4, this is due to the fact that the surface binding energy that sputtered particles must overcome to leave the bulk is subtracted from the particle's kinetic energy in the direction normal to the target surface, leading to a behavior similar to that of refraction.

As the energy of the incident particle increases, however, this phenomenon is reduced, as the sputtered particles have more than enough energy to be liberated from the target surface, and the distribution takes on a more characteristic cosine or Lambertian shape. Additionally, at low energies, if the incidence angle is increased from normal to grazing, the PDF becomes more "forward-scattered," leaning preferentially along the incident particle's trajectory. At certain angles, single-knock-on (SKO) peaks begin to arise; these are superimposed sharp peaks on top of the forward-scattered PDF, often close to the angle of specular reflectance of the incident projectile. The term "single-knock-on" refers to the fact that the ejected particle has received only a single collision or interaction with the incident ion, as opposed to multiple interactions that could lead to more complex energy distributions and PDFs. Beyond 1 keV, the directionality of the incident ion matters less, and the PDFs again take on a more Lambertian shape. These aforementioned PDF characteristics can be seen in Fig. 5.

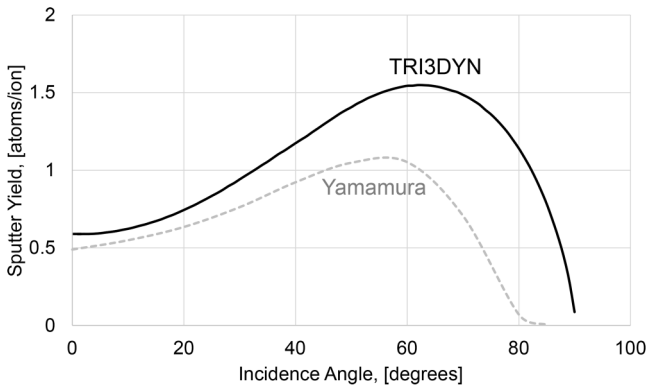


**FIG. 3.** Sputter yield increasing as a function of the ion incidence angle, generated from ion–solid interaction simulation TRI3DYN of 300 eV xenon impacting tungsten. Yamamura semi-analytical function is also plotted, showing general trend agreement.[34]

### C. Binary-collision approximation modeling

MD simulations excel in modeling ion–solid interactions near the sputtering threshold, where many-body effects are crucial, but they are computationally costly for large systems of atoms.[36] The "gold standard" for rapid modeling of low (100 eV) to high (100 keV) energy ion–solid interactions is through binary-collision approximation Monte Carlo simulations.[30] The premise revolves

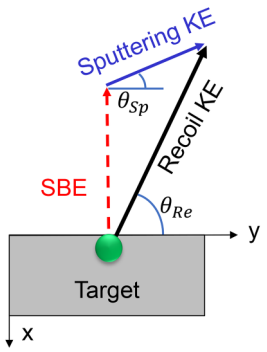


**FIG. 4.** The surface binding energy of a material dictates the sputter yield and influences the PDFs of sputtered particles to become under-cosine at low ion energies. At higher kinetic energies, the refraction effect becomes diminished, and PDFs become more Lambertian.

around computing scattering integrals for interactions between projectile–target pairs as they propagate through the bulk, modeling the transport of the initial projectile, recoil atoms, and sputtered particles. This process is completed for many instances of projectiles, allowing statistical distributions of sputter yield and sputterant trajectory to be formed.

Recent advancements in BCA codes have spawned versions that can simulate this process in three dimensions and can model the time-dependent evolution of the target material, thereby including compositional changes, such as surface morphology, ion implantation, and dislocations.[21,22] BCA simulations are often in better agreement with experimental results than analytical functions as they are well-positioned to capture phenomena that arise due to certain pairings of atomic species, rely less on rigid empirical frameworks, and include simulation parameters that can be altered to create models that align with experimental results.

## D. Available BCA solvers

There are a multitude of BCA software packages available to researchers, written in many different programming languages, each with their strengths and weaknesses. While there are a few BCA solvers that can simulate crystalline structures (e.g., MARLOWE[37]), most simulate amorphous targets.

### 1. Transport of ions in matter (TRIM)

TRIM, or the transport of ions in matter, is a ubiquitous BCA package that has received over 15 000 citations.[23] It has proven its utility in applications such as nuclear physics, plasma manufacturing, and semiconductor doping.[38–40] While it is easy to use, it has a number of drawbacks. The Ziegler–Biersack–Littmark interaction potential that TRIM employs has been found to be inadequate when modeling low-energy interactions and can provide sputter yields and sputterant PDFs that deviate substantially from experimental results.[25] Additionally, there are a number of programming issues embedded in the source-code of TRIM; namely, sputter yield is over-predicted at high angles of ion incidence, erroneous sputterant PDF profiles are produced for low Z targets ($Z \leq 14$), over-cosine PDFs are produced for high Z targets, and forward-directed distributions for grazing incidence projectiles are not reproduced.[25–28] Evidence of these computational shortcoming can be found in the Nadvornik *et al.* study,[24] wherein the characteristic cosine or Lambertian distribution was produced by TRIM, even at low energies and high ion incidence angles.

### 2. TRI3DYN

A more appropriate BCA solver designed to focus on accurate calculation of low-energy collisions and sputtering is known as TRIDYN.[41] It is a dynamic BCA algorithm that uses the Krypton–Carbon interaction potential[42] and includes changes to target stoichiometry due to embedded projectile atoms, atomic mixing, and preferential sputtering. A variant of TRIDYN that is able to model



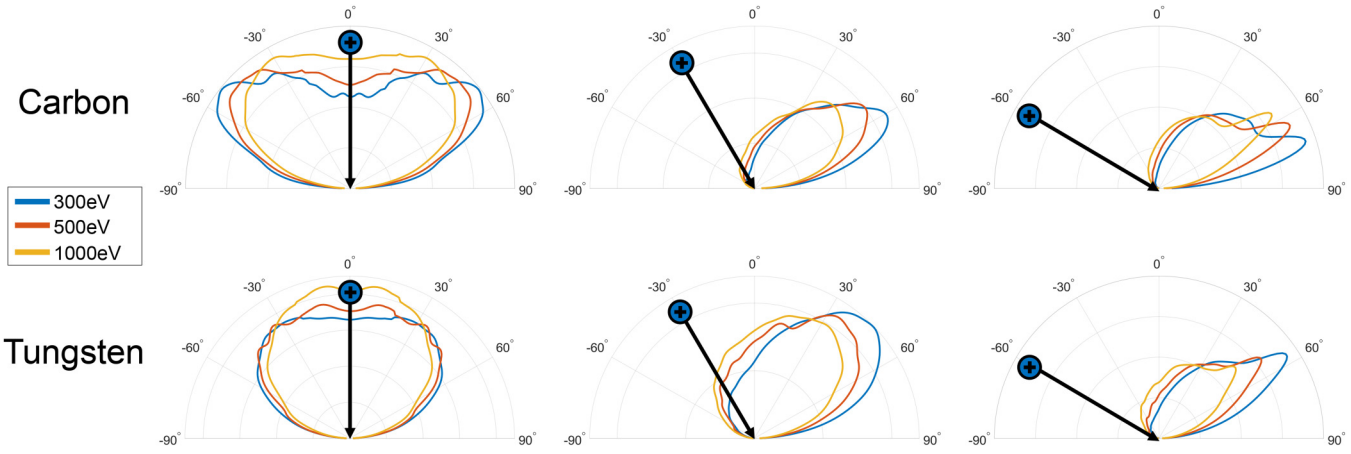


**FIG. 5.** PDFs for xenon ions impacting carbon and tungsten at varying ion incidence angles, collected from binary-collision approximation code, TRI3DYN. Note the prominent single-knock-on (SKO) peaks in the 60° incidence PDFs.

BCA processes for complex 3D geometries, called TRI3DYN, was used in this study, as it has been widely validated across experimental studies in the field of nuclear fusion, in low to medium-energy sputtering regimes.[21,43–45] Figure 6 shows time steps of a dynamic BCA simulation in TRI3DYN of a focused ion beam carving out a pocket in a target.

## III. METHODS

### A. Extracting sputter yield and PDF data

While it is possible to simulate large geometries in TRI3DYN, it is more computationally efficient to extract the relevant physics and create a faster, more extensible simulation environment for modeling plasma-exposed VCMs. Therefore, this section presents the process of using TRI3DYN to determine the relevant sputter characteristics of xenon ions impinging on carbon and tungsten. The datasets of sputter yield and PDF, as a function of energy and incidence angle, are extracted and processed; these metrics will be used to inform the governing equations of a simplified, particle-tracking simulation tool.

The precision of BCA solutions as a method of informing the governing particle dynamics is preferred over analytical functions, such as those popularized by Yamamura and Matsunami,[34] due to their ability to capture additional physics related to specific projectile-target material combinations, as well as higher order sputtering effects.

Figure 5 depicts the PDFs of flat, stochastically roughened amorphous carbon and tungsten—both low sputter yield materials that have seen use in fusion and space propulsion applications. Note that while the two materials produce slightly different PDF shapes, the same general features and trends can be seen. Namely, the shift from the under-cosine, butterfly distribution at 300 eV, moving toward a more uniform, cosine shape with higher energies, at normal incidence. Also, the forward-scattered distributions are clearly seen at 30° and 60° incidence, which become less distinct with increasing projectile energy. Lastly, SKO peaks can be seen at 60° incidence, becoming less prominent and shifting in location at higher incidence energies. In order to generate the PDFs from the raw data, hundreds of millions of entries of sputterant trajectory data are scraped, transformed, smoothed, and binned into a polar histogram. An example PDF in three-dimensions for a 30° incident, 300 eV xenon ion is shown in Fig. 7. The PDFs calculated from TRI3DYN show good agreement with experimental studies.[29]

The relationship between ion incidence angle, ion energy, and sputter yield for xenon impacting tungsten is shown in Fig. 8. The sensitive simulation parameter of surface binding energy was calibrated in order to produce sputter yields that compare well with experimental results. Note the peak in sputter yield occurs around 60°–70°, regardless of ion energy. Additionally, the sputter yield naturally increases with increasing ion energy, across all incidence angles.

These datasets of sputter yield and PDF can be substantially compressed compared to the raw data that was used to create them, allowing the conversion to smooth, interpolated functions for reduced-order VCM computational modeling tools.

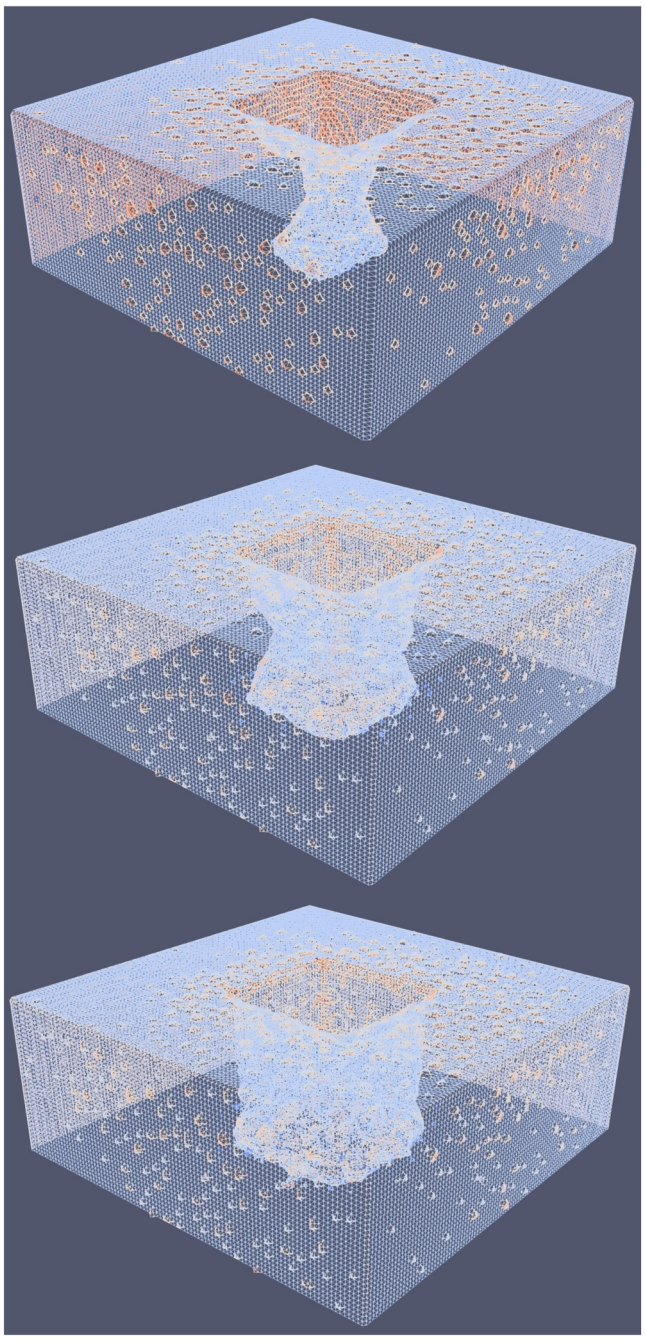

**FIG. 6.** 3D renderings of TRI3DYN simulation, using 20 keV xenon ions to perform a 20 × 20 Å focused ion beam (FIB) cut into a block of aluminum.

### B. Particle tracking computational model

A computational model based on particle-tracking was developed, enabling rapid simulation and iteration of three-dimensional VCM designs. Statistical distributions of PDF and sputter yield are

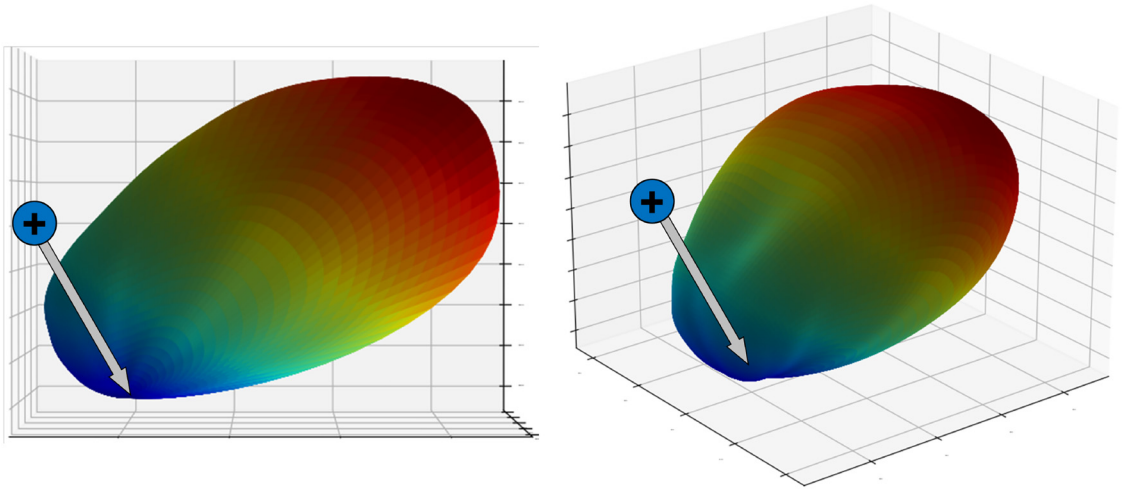

**FIG. 7.** 3D PDF of a 300 eV xenon ion impacting tungsten at 30°, pictured from side (left) and isometric (right) perspectives; note the strong forward bias of the sputtered particles. Surface color is plotted as probability magnitude and is calculated as the L2-norm from impact origin.

gathered from TRI3DYN BCA data to accurately simulate transport mechanisms through a Monte Carlo approach. This model has been implemented in the COMSOL particle-tracking computational environment, due to its ability to efficiently process large simulations. There is no inherent length scale to the simulation, as the ions and sputtered particles are treated as point particles, and the velocity of the particles is arbitrary; this allows simulation results to be valid across a range of geometric scales.

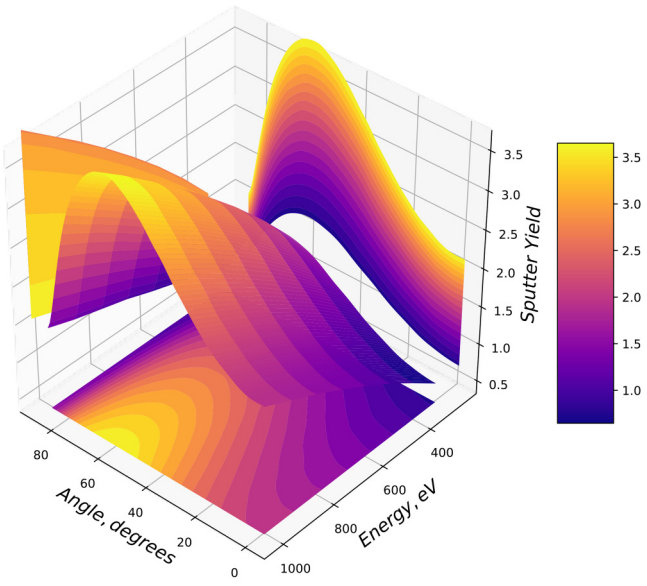


**FIG. 8.** Surface plot relating ion incidence angle, energy, and sputter yield of xenon impacting tungsten.

### C. Model description and sputtering physics

VCM geometries are generated in the computational domain, and impinging ions are directed normal to the structure at a single value of ion energy. Ions are introduced over an area equivalent to the size of one unit cell of the VCM under bombardment in order to reduce any effects of a non-infinite structure in the transverse directions. Upon interaction of ions with the structure, two separate calculations are performed. First, a weighted probability function is called that randomly determines the number of sputtered particles to be ejected from that impact event. This is due to the fact that, while the average sputter yield is a non-integer, only discrete numbers of particles are able to be simulated. Weighted probability distributions of sputter yield for all angles of ion incidence are stored in a database to be drawn upon. Figure 9 illustrates the statistical nature of the sputter yield function. These sputtered particles are then created and projected out from the surface to pass through the structure. The second computation that is performed is the determination of exit vectors for the sputtered particles, corresponding to a statistical distribution of the PDF, given the initial ion's incidence angle.

Sputtered particles then propagate throughout the VCM geometry until they reach another geometric feature. Once a feature is reached, they deposit and "stick" to the surface, as the sticking coefficient of sputtered particles in the literature has generally been found to be on the order of unity.[46,47] If large enough numbers of initial ions are generated, then the Monte Carlo nature of the model will produce final results for total sputtered particles and their locations that approach similar values across simulations. This model has been extensively validated and has been shown to produce identical PDFs and sputter yields that agree with the BCA data that inform the model.

The flexible framework and computational robustness of the particle-tracking environment is conducive to iterative refinement

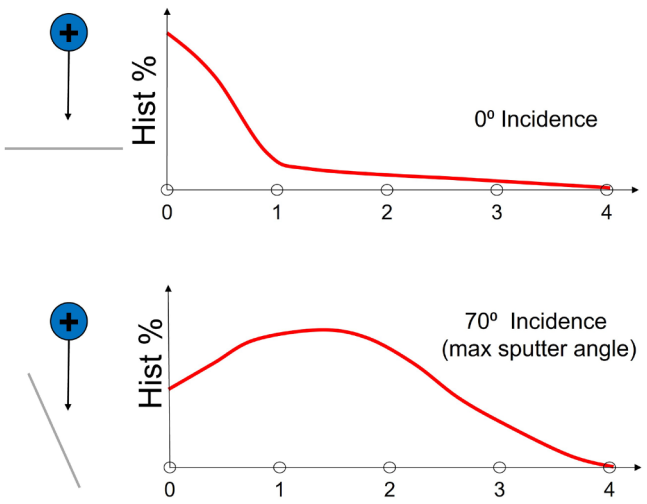


**FIG. 9.** A weighted probability function of angle-dependent sputter yield for 300 eV xenon impacting tungsten. Rather than utilizing the closest integer to the average sputter yield for a given incidence angle and ion energy, the simulation performs a random weighted selection from the yield histogram.

as it allows for rapid parametric optimization and analysis of potential sputter-resistant geometries. "Collectors" strategically placed on grouped surfaces within the model effectively aggregate essential statistics related to sputter yield, overall sputterant production, and ion transport mechanisms, streamlining the process of calculating objective functions and constraints.

## IV. RESULTS

In this section, a representative example of a candidate VCM geometry undergoing bombardment in a plasma-facing regime is presented. This case study showcases the ability of the particle-tracking simulation to model transport and sputtering physics in VCMs, providing insight into the mechanisms of erosion and self-healing.

### A. Representing stochastic VCM structures with Kelvin cells

To model existing stochastic foam VCM structures that have demonstrated reduced sputter yield by Li and Wirz,[6] arrays of Kelvin cells are simulated in the particle-tracking environment. Kelvin cells, shown in Fig. 10, are minimal-energy structures that approximate the average unit cell of stochastic metal foams.[48]

A Kelvin cell structure composed of tungsten, with geometry similar to that found in the Li and Wirz study was simulated; namely, 10 pores per inch (PPI), 8% density, as well as a higher density structure, 30%, for comparison. These targets are bombarded by xenon ions at 300 eV. While the VCM tested in the Li and Wirz experiment was aluminum bombarded by 300 eV argon ions, the PDFs of both material combinations are similar in character such that the results can be reasonably compared. Additionally, the relative sputter yields, $Y_{rel}$ (defined as the ratio of VCM sputter yield, $Y$, to flat sputter yield, $Y_0$) are compared to eliminate differences that exist between sputter yield magnitudes of Ar–Al and Xe–W. As a note, in this context, $Y$ refers to the ratio of sputtered particles that exit the upper surface of the VCM (i.e., the plasma-facing surface) to the number of incident ions.

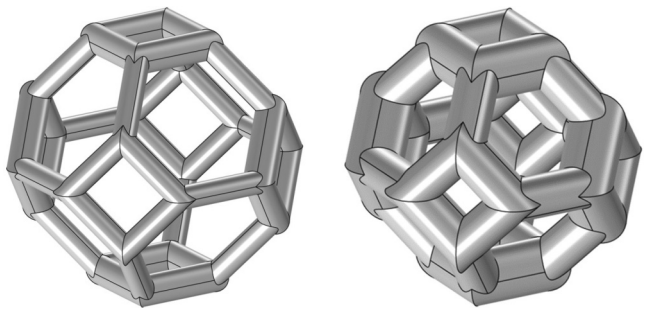

**FIG. 10.** Kelvin cells, 8% density (left) and 30% density (right). These structures are also known as tetrakaidecahedrons.

The structures are rotated 7° to eliminate ion transparency, removing unrealistic symmetry planes through which sputtered particles can channel through the structure unimpeded (see Fig. 11). The number of particles released into the structure was chosen to reduce the run-to-run difference in sputter yield to 1%; 10 000 particles were found to be adequate for the geometries in this study.

Table I summarizes the results of the particle-tracking simulation runs and the experimental data from Li and Wirz. In the simulation environment, the analogue geometry that is the closest to the Li and Wirz experiment (8% density), produces a $Y_{rel} = 0.447$,

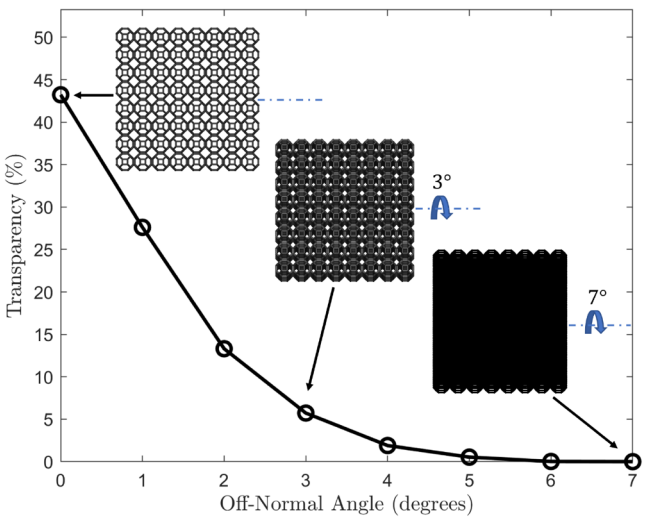


**FIG. 11.** Variation of VCM transparency as a function of rotation angle. At 8% VCM density, essentially all transparency is eliminated by 7° of rotation.

**TABLE I.** Comparison of sputter yields of the Li and Wirz VCM experiments and the particle-tracking model. The additional metric of inter-VCM yield highlights the enhanced production and subsequent deposition of sputtered material within the VCM.

| | Relative yield $[Y/Y_0]$ | Inter-VCM yield [Final ptcls./Initial ptcls.] |
|---|---|---|
| 6 | 0.4–0.6 | … |
| 8% Density | 0.447 | 1.13 |
| 30% Density | 0.636 | 1.19 |

whereas the higher density structure produced a slightly higher $Y_{rel} = 0.636$. Snapshots of these simulations are shown in Figs. 12 and 13. This increased value of $Y_{rel}$ is due to the thicker ligaments on the upper layers projecting more sputtered particles out of the top surface of the VCM. The simulation results largely fall within the experimental findings, supporting the validity of the model.

Inter-VCM yield, defined as the ratio of the total number of final sputtered particles to incident ions (regardless of if they exit the top surface of the VCM or remain in the structure), was also calculated, also shown in Table I. In both geometries, the VCMs have a inter-VCM yield greater than one, indicating that the ions produce substantial "damage" to the structure, but the majority of the sputtered particles that are created become geometrically trapped in the VCM. Altering the angle of the VCM in the simulation produced sputter yields that varied roughly 5% from the presented values, as long as the transparency of the VCM was still zero.

### B. Ion transport phenomenology

In plasma-facing conditions, where ions sputter only from the top of VCM ligaments, the shape of the ligament's upper surface determines the overall transport of sputtered particles. By examining an amalgamation of PDFs across curved surfaces, it can be found that circular ligaments give rise to fewer sputtered particles that exit the VCM compared to a flat surface; although more sputtered particles are created overall, the edges of the circular ligament produce amalgamated sputterant PDFs that are directed downward into the VCM. Examples of amalgamated

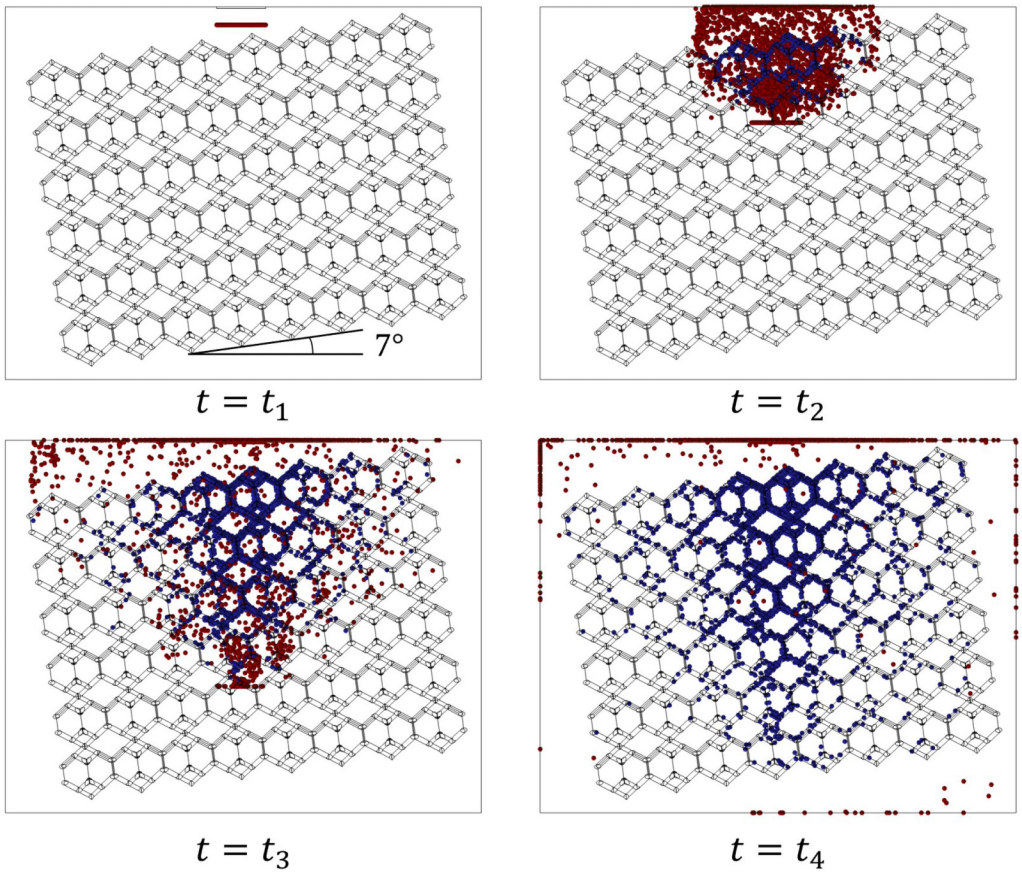


**FIG. 12.** Side view of the 8% density Kelvin cell structure, illustrating time evolution of sputtered particles transport throughout the geometry. Red particles indicate sputtered particles that have left the VCM, while blue indicate geometrically trapped particles.

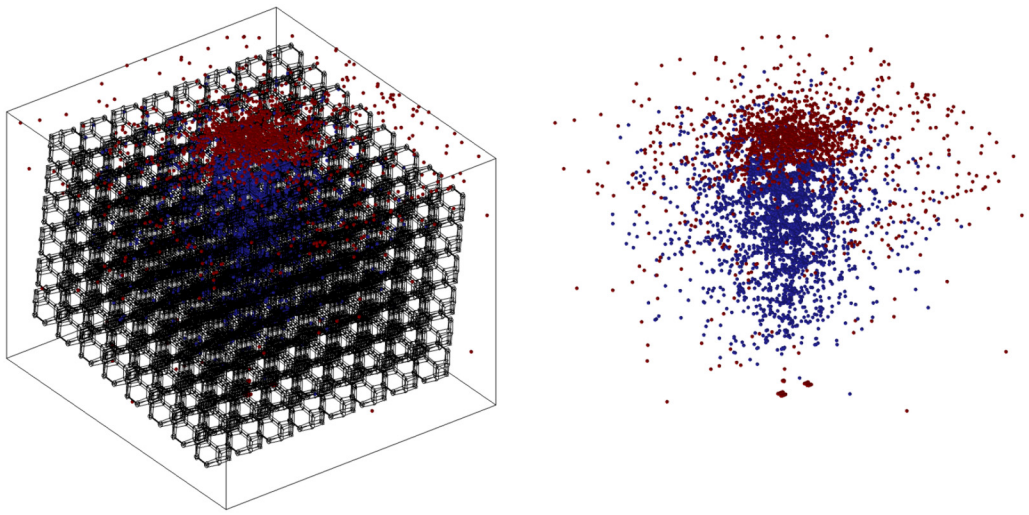

**FIG. 13.** Isometric view of sputtered particles in 8% density Kelvin cell. Left: Pictured with mesh outline. Right: Without mesh outline.

PDFs of a single, circular, plasma-facing ligament is shown in Fig. 14. Note that the large forward sputtered lobes on either side of the ligament are primarily due to increased sputter yield at grazing incidence angles.

The pronounced downward transport shown by the amalgamated PDFs is at the core of the ability of VCMs to resist sputtering erosion. By sending material from upper layers to lower layers, the material that would be lost to the plasma in the case of flat surfaces can recombine with lower areas of the VCM, eventually sputtering again at a later point in the VCM's evolution. Additionally, sputtered particles that are projected in an upward direction can be captured on the underside of the ligaments above them, increasing ligament diameter and thereby contributing to the self-healing of structures that are eroded from the plasma-facing side. This opens up the opportunity to explore ligament shapes with varying surface topography to more precisely control the transport of sputtered particles. Indeed, across the virtually unbounded design space of VCM parameters, there likely exist geometries that can be designed to recirculate material throughout the VCM more efficiently than those shown in this study.

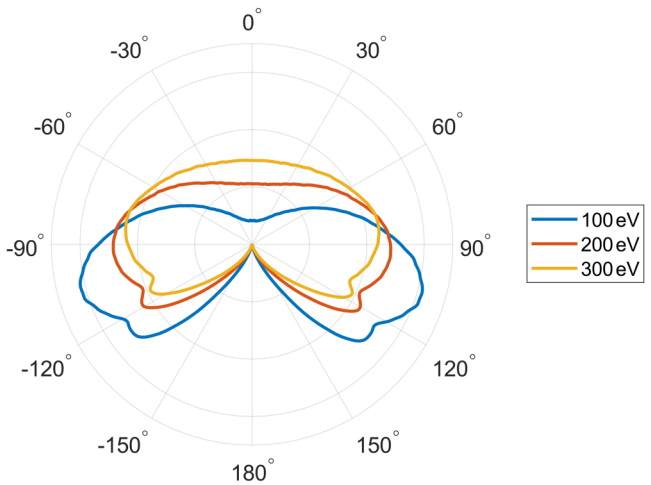


**FIG. 14.** Amalgamated ligament PDFs for a single circular tungsten ligament, impacted by xenon ions at various energies. PDFs are normalized to one another for clarity of presentation; in reality, higher energy ions produce amalgamated PDFs with larger areas.

## V. CONCLUSION

Multi-scale modeling informed by BCA data and implemented in a particle-tracking environment has provided insightful characterization of VCMs in plasma-facing conditions. The particle tracking simulation results showcased that a sputter yield reduction is in close agreement with experimental studies, reaffirming the robustness of the simulation model. Furthermore, our exploration of the phenomenology of ion transport revealed key insights into how VCM geometries could be optimized for better sputtering resistance. The role of ligament shapes in determining sputterant behavior was found to be particularly influential, highlighting an additional avenue for material design optimization. Future research will incorporate time-dependent sputter yields, self-sputtering, and back-scattered ions. Additional parameters such as the pore size, ligament size and shape, material composition, and gradients of these parameters as a function of layer number will also be probed to determine their influence on sputter minimization efforts. This study is intended to serve as a fundamental contribution to ongoing efforts in optimizing material systems for plasma exposure, with the objective of advancing the fields of fusion energy and space propulsion systems.

## ACKNOWLEDGMENTS

This work was supported by the Advanced Research Projects Agency - Energy (ARPA-E) DE-AR0001378 for the Advanced Materials for Plasma Exposed Robust Electrodes (AMPERE) Project.

## AUTHOR DECLARATIONS

### Conflict of Interest

The authors have no conflicts to disclose.

### Author Contributions

**Graeme Sabiston:** Conceptualization (equal); Data curation (lead); Formal analysis (lead); Investigation (equal); Methodology (equal); Software (lead); Validation (lead); Visualization (lead); Writing – original draft (lead); Writing – review & editing (equal). **Richard E. Wirz:** Conceptualization (equal); Funding acquisition (lead); Investigation (equal); Methodology (equal); Project administration (lead); Resources (lead); Supervision (lead); Writing – review & editing (equal).

## DATA AVAILABILITY

The data that support the findings of this study are available from BCA software TRI3DYN, licensed by Helmholtz-Zentrum Dresden-Rossendorf (HZDR) Research Facility. Restrictions apply to the availability of these data, which were used under license for this study. Data are available from the corresponding author upon reasonable request and with the permission of HZDR.

## REFERENCES

[1]J. Knaster, A. Moeslang, and T. Muroga, Nat. Phys. **12**, 424–434 (2016).
[2]B. Wirth, K. Nordlund, D. Whyte, and D. Xu, MRS Bull. **36**, 216–222 (2011).
[3]I. Levchenko, K. Bazaka, T. Belmonte, M. Keidar, and S. Xu, Adv. Mater. **30**, 1802201 (2018).
[4]J. Polk, A. Kelly, R. Jahn, H. Kurtz, and M. Auweter-Kurtz, "Mechanisms of hot cathode erosion in plasma thrusters," in *21st International Electric Propulsion Conference* (Electric Rocket Propulsion Society, 1990), p. 2673.
[5]R. Behrisch and W. Eckstein, *Sputtering by Particle Bombardment* (Springer-Verlag, New York, 1981), Vol. 1.
[6]G. Z. Li and R. E. Wirz, Phys. Rev. Lett. **126**, 035001 (2021).
[7]G. T. Sabiston and R. E. Wirz, "Thrust densification of space electric propulsion systems via volumetrically complex materials," in *AIAA SCITECH 2024 Forum* (American Institute of Aeronautics and Astronautics, Inc., 2024), p. 1136.
[8]G. Sabiston and R. Wirz, "Sputtering reduction optimization via volumetrically complex materials," *APS Division of Plasma Physics Meeting Abstracts, January 2022*, APS Meeting Abstracts, GP11.089 (SAO/NASA Astrophysics Data System, 2022), Vol. 2022, pp. GP11.089, available at: https://ui.adsabs.harvard.edu/abs/2022APS..DPPGP1089S
[9]G. Sabiston and R. Wirz, "Optimization of additively manufactured plasma-facing surfaces with consideration of plasma infusion effects," *APS Division of Plasma Physics Meeting Abstracts, January 2023*, APS Meeting Abstracts, PP11.132 (SAO/NASA Astrophysics Data System, 2023), Vol. 2023, pp. PP11.132, available at: https://ui.adsabs.harvard.edu/abs/2023APS..DPPPP1132S
[10]A. Ottaviano, R. Wirz, G. Wan, G. Sabiston, M. Konopliv, and A. Thuppul, "Persistent sputtering yield reduction in plasma-infused materials for plasma propulsion and fusion," *APS Division of Plasma Physics Meeting Abstracts, January 2022*, APS Meeting Abstracts, UO08.009 (SAO/NASA Astrophysics Data System, 2022), Vol. 2022, pp. UO08.009, available at: https://ui.adsabs.harvard.edu/abs/2022APS..DPPUO8009O
[11]C. E. Huerta and R. E. Wirz, AIP Adv. **9**, 125009 (2019).
[12]C. Huerta, T. Matlock, and R. Wirz, J. Appl. Phys. **119**, 113303 (2016).
[13]M. Patino and R. Wirz, Appl. Phys. Lett. **113**, 041603 (2018).
[14]A. Ottaviano, "Plasma interactions and electron dynamics for volumetrically complex materials," Ph.D. thesis (University of California, Los Angeles, 2023).
[15]C. Anders, E. M. Bringa, and H. M. Urbassek, Nucl. Instrum. Methods Phys. Res., Sect. B **342**, 234–239 (2015).
[16]H. Tran and H. Chew, Carbon **205**, 180–193 (2023).
[17]P. Brault, Front. Phys. **6**, 59 (2018).
[18]A. Lopez-Cazalilla, J. Jussila, K. Nordlund, and F. Granberg, Comput. Mater. Sci. **216**, 111876 (2023).
[19]A. Sycheva, E. Voronina, T. Rakhimova, and A. Rakhimov, Appl. Surf. Sci. **475**, 1021–1032 (2019).
[20]Y. G. Li, Y. Yang, M. P. Short, Z. J. Ding, Z. Zeng, and J. Li, Sci. Rep. **5**, 18130 (2015).
[21]W. Möller, Nucl. Instrum. Methods Phys. Res., Sect. B **322**, 23–33 (2014).
[22]A. Mutzke, R. Schneider, W. Eckstein, R. Dohmen, K. Schmid, U.v. Toussaint, and G. Badelow, SDTrimSP version 6.00, IPP Report 2019/02, MaxPlanck-Institut fr Plasmaphysik, 2019, available at: https://scholar.google.com/scholar?cluster=6434671027804546925&hl=en&as_sdt=2005&sciodt=0,5
[23]J. F. Ziegler, M. D. Ziegler, and J. P. Biersack, Nucl. Instrum. Methods Phys. Res., Sect. B **268**, 1818–1823 (2010).
[24]W. Nadvornick, H. Y. Chang, A. Alvarado, P. Molina, J. Marian, and N. Ghoniem, J. Nucl. Mater. **553**, 153010 (2021).
[25]H. Hofsäss, K. Zhang, and A. Mutzke, Appl. Surf. Sci. **310**, 134–141 (2014).
[26]V. Shulga, Appl. Surf. Sci. **439**, 456–461 (2018).
[27]K. Wittmaack, J. Appl. Phys. **96**, 2632–2637 (2004).
[28]K. Wittmaack, Nucl. Instrum. Methods Phys. Res., Sect. B **380**, 57–70 (2016).
[29]K. A. Zoerb, J. D. Williams, D. D. Williams, and A. P. Yalin, "Differential sputtering yields of refractory metals by xenon, krypton, and argon ion bombardment at normal and oblique incidences," *29th International Electric Propulsion Conference, October 2005* (Electric Propulsion Rocket Society, 2005), pp. 2005–293.
[30]W. Eckstein, *Computer Simulation of Ion-Solid Interactions* (Springer Science & Business Media, 2013), Vol. 10.
[31]M. T. Robinson, Radiat. Eff. Defects Solids **130**, 3–20 (1994).
[32]P. Sigmund, Phys. Rev. **184**, 383 (1969).
[33]K. B. Cheney and E. T. Pitkin, J. Appl. Phys. **36**, 3542–3544 (1965).
[34]Y. Yamamura, Y. Itikawa, and N. Itoh, Report IPPJ-AM-26, Institute of Plasma Physics, Nagoya University (1983).
[35]Y. Yamamura, Radiation Effects **55**, 49–55 (1981).
[36]H. M. Urbassek, Nucl. Instrum. Methods Phys. Res., Sect. B **122**, 427–441 (1997).
[37]M. T. Robinson and I. M. Torrens, Phys. Rev. B **9**, 5008 (1974).
[38]R. E. Stoller, M. B. Toloczko, G. S. Was, A. G. Certain, S. Dwaraknath, and F. A. Garner, Nucl. Instrum. Methods Phys. Res., Sect. B **310**, 75–80 (2013).
[39]M. Kumar, T. Kumar, R. K. Pandey, S. Pathak, R. Kumar *et al.*, Mater. Lett. **303**, 130474 (2021).
[40]A. Nipane, D. Karmakar, N. Kaushik, S. Karande, and S. Lodha, ACS Nano **10**, 2128–2137 (2016).
[41]W. Möller and W. Eckstein, Nucl. Instrum. Methods Phys. Res., Sect. B **2**, 814–818 (1984).
[42]W. Wilson, L. Haggmark, and J. Biersack, Phys. Rev. B **15**, 2458 (1977).
[43]R. Stadlmayr, P. Szabo, D. Mayer, C. Cupak, W. Möller, and F. Aumayr, Phys. Scr. **2020**, 014021 (2020).
[44]R. Stadlmayr, P. Szabo, D. Mayer, C. Cupak, T. Dittmar, L. Bischoff, S. Möller, M. Rasiński, R. Wilhelm, W. Möller, and F. Aumayr, J. Nucl. Mater. **532**, 152019 (2020).
[45]R. Stadlmayr, "Erosion of fusion relevant materials-experiments and modelling," Ph.D. thesis (Technische Universität Wien, Wien, 2020).
[46]T. Nakano and S. Baba, Vacuum **80**, 647–649 (2006).
[47]B. Emmoth and H. Bergsaker, Nucl. Instrum. Methods Phys. Res., Sect. B **33**, 435–437 (1988).
[48]W. Y. Jang, S. Kyriakides, and A. M. Kraynik, Int. J. Solids Struct. **47**, 2872–2883 (2010).